JACS
JOURNAL OF THE AMERICAN CHEMICAL SOCIETY
Article
Cite This: J. Am. Chem. Soc. 2018, 140, 940−946
pubs.acs.org/JACS

Large Converse Piezoelectric Effect Measured on a Single Molecule on a Metallic Surface

Oleksandr Stetsovych,[†] Pingo Mutombo,[†] Martin Švec,[†,‡] Michal Šámal,[§] Jindřich Nejedlý,[§] Ivana Císařová,[∥] Héctor Vázquez,[†] María Moro-Lagares,[†,‡] Jan Berger,[†] Jaroslav Vacek,[§] Irena G. Stará,[§] Ivo Starý,*[,§] and Pavel Jelínek*[,†,‡]

[†]Institute of Physics of the Czech Academy of Sciences, Cukrovarnická 10, 18221 Prague 6, Czech Republic
[‡]Regional Center of Advanced Technologies and Materials, Palacký University, 77147 Olomouc, Czech Republic
[§]Institute of Organic Chemistry and Biochemistry, Czech Academy of Sciences, Flemingovo nám. 2, 16610 Prague 6, Czech Republic
[∥]Department of Inorganic Chemistry, Faculty of Science, Charles University in Prague, Hlavova 2030/8, 12843 Prague 2, Czech Republic

Supporting Information

ABSTRACT: The converse piezoelectric effect is a phenomenon in which mechanical strain is generated in a material due to an applied electrical field. In this work, we demonstrate the converse piezoelectric effect in single heptahelicene-derived molecules on the Ag(111) surface using atomic force microscopy (AFM) and total energy density functional theory (DFT) calculations. The force−distance spectroscopy acquired over a wide range of bias voltages reveals a linear shift of the tip−sample distance at which the contact between the molecule and tip apex is established. We demonstrate that this effect is caused by the bias-induced deformation of the spring-like scaffold of the helical polyaromatic molecules. We attribute this effect to coupling of a soft vibrational mode of the molecular helix with a vertical electric dipole induced by molecule−substrate charge transfer. In addition, we also performed the same spectroscopic measurements on a more rigid *o*-carborane dithiol molecule on the Ag(111) surface. In this case, we identify a weaker linear electromechanical response, which underpins the importance of the helical scaffold on the observed piezoelectric response.

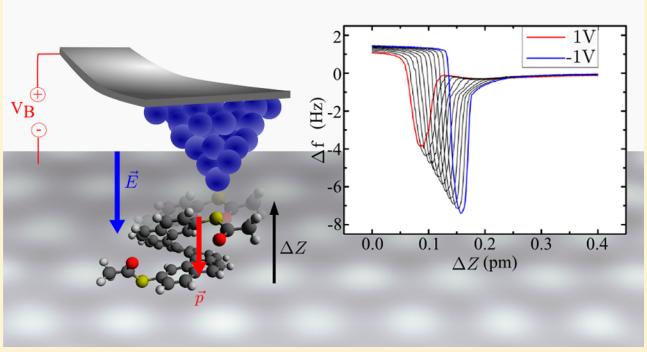

1. INTRODUCTION

Piezoelectric effect (PE) emerges in materials in which the mechanical and electrical degree of freedom are coupled. Either the electric field can be reversibly generated if a mechanical stress is applied (direct PE) or, conversely, the mechanical strain can arise if the electric field is applied (converse PE). Materials endowed with such a property have to be noncentrosymmetric, poorly conductive and the magnitude of their dipole moment is altered under the mechanical stress. Many materials have been demonstrated to exhibit PE such as piezoelectric ceramics (lead zirconate titanate, PZT), polymers (polyvinylidene difluoride, PVDF) or quartz. They are central to a large number of applications in the automotive, computer, smartphone, consumer, medical and military industries.[1] Nowadays, new challenges have emerged in the context of PE to realize self-powered devices or dramatically reduce their size indispensable for a nanoscale use.[2−6] Also, biological materials such as collagen fibrils,[7] proteins[8] or bacteriophages[9] show piezoelectric properties. In the quest for molecular nanoelectromechanical systems[10,11] there is a particular interest in designing single-molecule piezoelectric devices and demonstrating their function. Such an achievement has so far remained elusive despite the realization of single-molecule devices ranging from the diode,[12] transistor,[13] resonant tunneling junction,[14] thermoelectric junction,[15] rotor,[16] unidirectional motor,[17−20] molecular machine,[21] artificial muscle[22] to nanocars[23,24] that have already been reported.

Inherently chiral helicenes (helical all-*ortho*-annulated polyaromatics)[25] are promising candidates as piezoelectrically active molecules. They lack inversion symmetry, possess a spring-like carbon scaffold exhibiting an extraordinary deformation capacity (when compressed/stretched along the helix axis)[26−31] and can be functionalized by electronically distinguished moieties at their opposite termini to install a properly oriented dipole moment. Within this scenario, Hutchison et al. theoretically analyzed a set of asymmetrically substituted [6]helicenes and their analogues equipped with various electron donating and withdrawing groups varying also the polarizability of their backbones.[32] Importantly, they

Received: August 23, 2017
Published: December 23, 2017

DOI: 10.1021/jacs.7b08729
J. Am. Chem. Soc. 2018, 140, 940−946

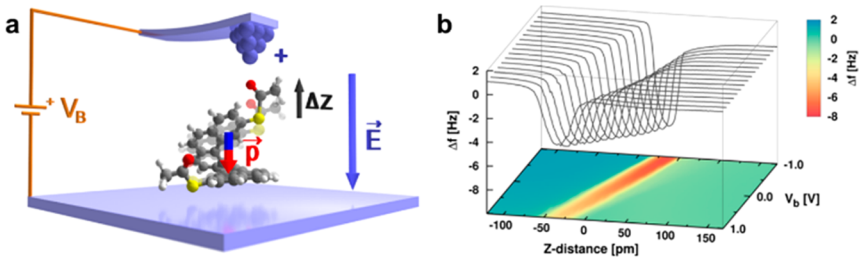

Figure 1. Measurements of the piezoelectric effect on the molecule 7HdiET by AFM. (a) Ball-and-stick model of the experiment. (b) Measured $\Delta f(z,V_B)$ for the single molecule 7HdiET with the same tip: the frequency shift Δf vs z-distance spectroscopies acquired for different bias voltages V_B.

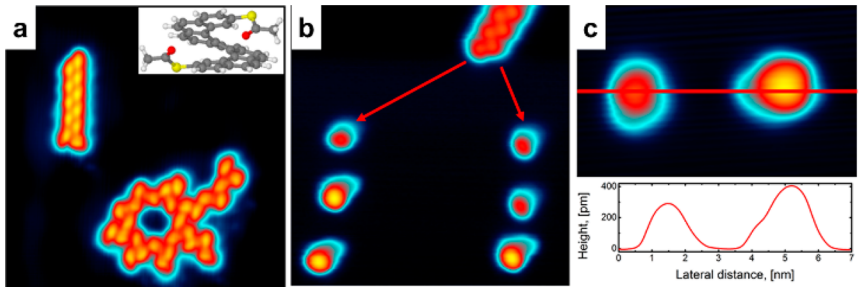

Figure 2. Molecules 7HdiET on the Ag(111) surface. (a) STM overview image of self-assemblies of 7HdiET on Ag(111). Each bright protrusion corresponds to one molecule. Inset: a ball-and-stick model of 7HdiET. (b) STM image of a partially reassembled island by scanning probe manipulation. Red arrows highlight the direction of single molecules displacement . Molecules, after manipulation process, stabilize in two different conformations that can be distinguished by their different apparent height in STM. (c) STM line profile over two molecules in different conformations. Images taken at 5 K, (a) I_t = 10 pA, V_b= 30 mV, image size: 18 × 18 nm^2; (b) I_t = 5 pA, V_b = 1 V, image size: 15 × 15 nm^2; (c) I_t = 10 pA, V_b = 1.5 V, image size: 7 × 4.3 nm^2.

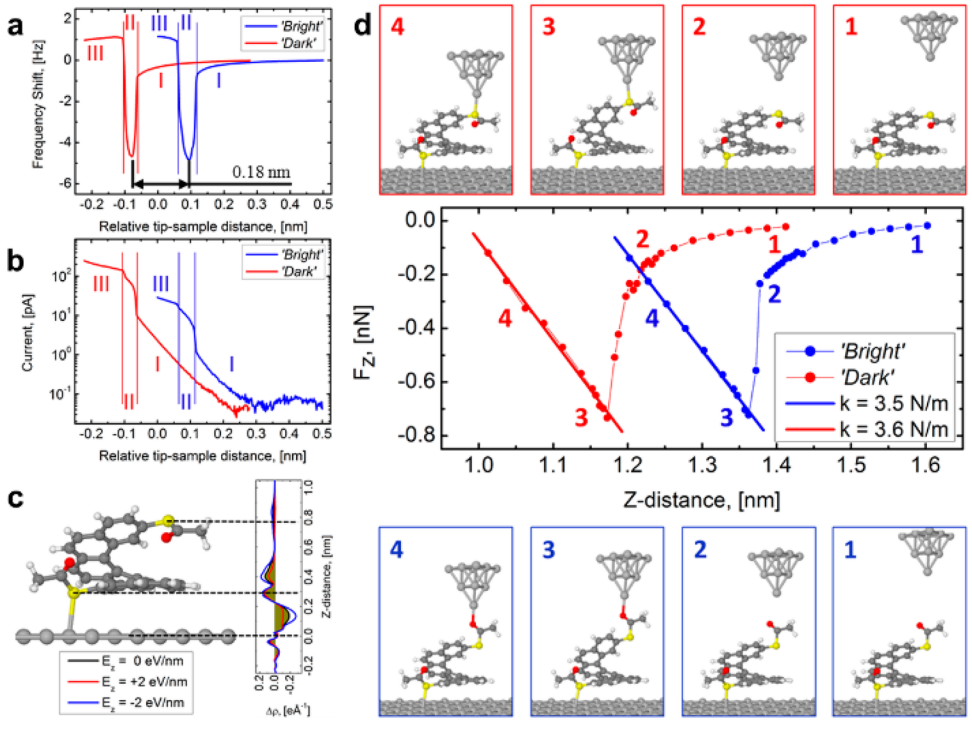

Figure 3. Contacting the molecules 7HdiET in bright and dark conformations. (a) Frequency shift and (b) simultaneously recorded tunneling current for bright (blue curve) and dark (red curve) conformers. Three characteristic regimes are marked. Regime I: the approach before the contact; regime II: forming and breaking the contact every oscillation cycle; regime III: the stable contact. The bright conformer is contacted at the higher tip sample distance (about ∼0.18 nm) than the dark one. Spectra are taken at 40 pm oscillation amplitude of the sensor. (c) Calculated 1D plot of the differential electron density ($\Delta\rho = \rho_{all} - \rho_{surf} - \rho_{mol}$) transfer between the molecule 7HdiET and Ag(111) surface for different external electric fields. (d) Calculated force vs distance curves for the molecules in bright and dark conformations, which reveal a linear regime after the contact. Numbers correspond to the tip−sample separations presented in the ball-and-stick model insets.

DOI: 10.1021/jacs.7b08729
J. Am. Chem. Soc. 2018, 140, 940−946

identified highly responsive helicene molecules that were foreseen to yield large piezoelectric coefficients in the range of tens to hundreds of pm/V (surpassing PVDF and competing with PZT). Thus, a successful development of the single-molecule piezoelectrics would enable a bottom-up approach to nanoelectromechanical systems such as molecular actuators (linear motors), sensors and electricity generators. A significant milestone on the pathway to realizing single-molecule piezoelectrics was the scanning tunneling microscopy (STM) study by Kimura et al. describing a two-state switching of the conductance and molecular length of dodecapeptide helix bundles immobilized on gold that was stochastic with time.[33] A correlation between the helix dipole moment orientation, polarity of applied bias and conformational changes of helices was demonstrated.

2. RESULTS AND DISCUSSION

Here, we report large electromechanical response of single molecules on surfaces that was observed on racemic heptahelicene derivatives (*S*,*S*′-heptahelicene-2,17-diyl diethanethioate, 7HdiET and heptahelicene-2,17-dithiol, 7HdiT) deposited on the Ag(111) surface by employing STM and atomic force microscopy (AFM) measurements. Namely, we performed simultaneous STM/AFM spectroscopic measurements over a wide range of the tip−sample distances and bias voltages, as shown schematically in Figure 1a. The force−distance spectroscopies (see Figure 1b) reveal a strong linear shift in the distance at which the molecule is contacted by the metallic tip, strongly dependent on the applied bias voltage. The experimental data allowed the determination of the single-molecule piezoelectric coefficient d_{33} of 7HdiET and 7HdiT to be ∼55 and ∼80 pm/V, respectively. We attribute this effect to the presence of an intrinsic dipole coupled with a soft vibrational mode of the helix scaffold. The intrinsic dipole moment parallel to the axis of the molecule helix, see Figure 1a, originates from charge transfer from the molecule to the metallic surface. In addition, we carried out control spectroscopic measurements on 1,2-dithiol-*ortho*-carborane (CBdiT) molecules, which have a rigid skeleton, on Ag(111). In this case, we identify a non-negligible but much weaker linear electromechanical response, which confirms the decisive influence of the helical scaffold on the electromechanical response.

Figure 2a shows the STM image of the racemic 7HdiET adsorbed on the Ag(111) surface at a temperature of 5 K. The molecules assemble into linear and circular islands or their combinations. From analysis of STM images and total energy DFT simulations, we identify that the molecules adopt face-on adsorption geometry, as shown on Figure 1a. We can deliberately disassemble the molecular islands via tip interactions with single molecules, as shown in Figure 2b. Individual molecules stabilize with two different conformations of the upper acetylsulfanyl group (distant from the Ag surface) that can be distinguished by the different apparent height of the molecule in the STM channel (see Figure 2c). We define the two conformers as "bright" and "dark" ones according to their appearance in the STM mode.

We can reversibly switch between the bright and dark conformers via a mechanical action with the tip or applying a positive bias voltage, see Figure S3. From DFT calculations we estimated that the dark conformer (Figure 3d) corresponds to an energetically slightly more stable structure (∼70 meV, see Figure S2), in which the oxygen atom of the upper acetylsulfanyl group points toward the Ag surface. This dark conformer can be converted, after the mechanical contact and subsequent tip retraction, to the bright conformer, in which the acetylsulfanyl group is rotated placing the oxygen atom outward the surface (Figures S3 and S4). Conversely, the bright conformer can be reproducibly switched to the dark conformer by the application of the positive bias voltage inducing repulsive electrostatic interaction between negatively charged tip and oxygen atom. Details of the switching mechanism are described in Supporting Information (see Supplementary Discussion).

Both of the molecular conformers can be contacted very reproducibly with a metallic tip. Figure 3a represents a characteristic evolution of the frequency shift Δf and simultaneously recorded tunneling current I_t during the tip approach over the dark and bright conformers. Such a simultaneous acquisition of the $\Delta f(z)$ and $I_t(z)$ spectroscopy allows us to monitor the process of contacting molecules in detail (Figure 3a,b). Qualitatively, it shows very similar features regardless of the fact whether bright or dark conformers are contacted. At far tip−sample distances (regime I), the tunneling current I_t increases exponentially, while the frequency shift Δf shows a quadratic dependence on applied bias voltage (see Figure S7 and related Supplementary Discussion in Supporting Information). Regime I corresponds to the tunneling regime where the molecule is not yet contacted. At a certain distance (regime II), we observe a sharp characteristic minimum in the frequency shift Δf being accompanied by a jump-like increase in the tunneling current I_t. It is worth noting that the width of the regime II is closely related to the oscillation amplitude (see Figure S8 in Supplementary Discussion). Regime II corresponds to the distance where the metallic tip apex is continuously establishing and breaking a chemical bond with the molecule in each oscillation cycle. Thus, we define the contacting distance z_c as the tip−sample distance at which the minima of the frequency shift occur. Approaching the molecule further (regime III), the frequency shift Δf stabilizes at positive values, while the tunneling current I_t returns to the exponential growth (at a lower rate than in the regime I). Consequently, the regime III corresponds to the tip−sample distance where the molecule maintains chemical contact with the tip.

The contacting distance of the molecules 7HdiET occupying the bright conformation is about 0.18 nm higher than that one in the dark conformer (Figure 3a). This difference can be rationalized by the outward orientation of the oxygen atom of the acetylsulfanyl group in the bright conformer. To corroborate this scenario, we performed the total energy DFT simulation of the process of approaching a metallic tip over both the oxygen and sulfur atom of the acetylsulfanyl group in the bright and dark conformation, respectively. The evolution of the interaction force between the tip and the molecule during the approach and corresponding structural changes are shown in Figure 3d. According to the DFT calculations, most of the structural deformation during the contact is related to vertical changes in the helical pitch but not affecting the Ag−S bond length (see Figure S13). The contacting occurs at a distance where a sharp decrease of the interaction force appears, see point 3 in Figure 3d. The calculated height difference of the contact distance z_c for the bright or dark conformer is about 0.189 nm, which is in a good agreement with the experimental value. It is worth noting that the current after the contact is about five times larger for the dark conformer than for the bright one. This experimental observation matches well with the calculated transmission

DOI: 10.1021/jacs.7b08729
J. Am. Chem. Soc. 2018, 140, 940−946

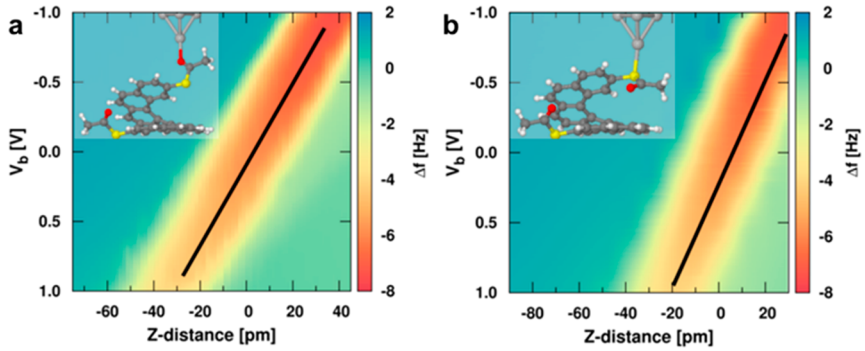

Figure 4. Piezoelectric response of 7HdiET molecule in bright and dark conformations. $\Delta f(z,V_B)$ maps recorded for the molecule 7HdiET in the (a) bright and (b) dark conformation. Positions of the minima of the frequency shift (highlighted with a black line) correspond to the contacting distances between the scanning probe tip and molecule. The relative contacting distance z_c changes with the applied sample bias indicating the piezoelectric deformation of the molecule with the applied electric field. The respective ball-and-stick contacting models are in the insets.

spectra[34,35] of both conformers in the contact regime (for more details, see Figures S9 and S10).

The recorded $\Delta f(z)$ spectra over different molecules with the same tip are well reproducible, as shown in Figure S12, demonstrating the formation of a well-defined molecular junction. Interestingly, in the regime III, the frequency shift Δf remains almost constant, especially when acquired with very low oscillation amplitude, see as shown in Figure S8. This means that the molecular junction acts as a linear spring. Indeed, structural deformations obtained from the total energy DFT calculations mostly consist of linear changes of the helix pitch in this regime for both conformers. Hence, an effective stiffness k_M of the helical spring can be directly estimated from the $\Delta f(z)$ spectroscopy. In the small amplitude regime, the effective stiffness k_M of the molecular junction can be calculated as $k_M = \Delta f \cdot 2k/f_o$, where $k = 1.08 \times 10^6$ N/m is the sensor stiffness, $f_o = 0.98$ MHz its eigenfrequency and the $\Delta f = 1.60 \pm 0.39$ Hz (measured from the $\Delta f(z)$ spectra taken from contacting 24 different bright conformers with the same tip, see Figure S12). Accordingly, we calculate the molecular spring constant k_M to be 3.53 ± 0.86 N/m. This value concurs very well with the effective stiffness estimated from the tip-molecule force on contact from DFT simulations: 3.6 ± 0.1 N/m. In addition, experimental inelastic electron tunneling spectroscopy reveals the presence of a soft vibrational mode (Figure S11a), which we tentatively relate to the breathing vibrational mode of the helix (Figure S11b). We should note that the calculated stiffness of Ag−S bond is 43 N/m, which is one order of magnitude higher then the stiffness of the helix. Consequently, structural deformation of the 7HdiET molecule by external stimuli takes place predominantly on the helical scaffold (Figure S13).

Next, we analyze charge transfer between the metal and molecule, which is expected to reflect both the Pauli repulsion and misalignment of energy bands of silver with energy levels of interacting molecular orbitals.[40,41] Therefore, we performed Kelvin probe force microscopy measurements to determine the electron transfer from the molecule 7HdiET to the metallic substrate. The $\Delta f(V_B)$ spectra (Figure S5) reveal a significant variation between the local contact potential difference V_{cpd} acquired over the 7HdiET molecule and on the bare Ag(111) substrate. In addition, we observe a shift of V_{cpd} above the molecule 7HdiET toward the higher values (from −0.70 to −0.48 V). This shift indicates the presence of an extra dipole moment oriented with its positive pole pointing to the surface as shown in Figure 1a. The origin of this vertical dipole moment can be understood as a consequence of the charge transfer from the molecule to the surface, in good agreement with the total energy calculations, see Figure 3c. Such a π-electron density rearrangement creates a positive charge at the helix terminus closer to the surface. Consequently, another dipole moment is created within the molecule helix. This internal molecular dipole is created by interaction of the positive charge at the helix terminus near the surface with an electron-rich terminal group (acetylsufanyl or thiol group) located at the opposite helix terminus. This dipole pointing downward is mainly sensed by the Kelvin probe in the far distance. Moreover, the presence of the dipole is also supported by the direction of vertical relaxation of the helix in the presence of the external electrostatic field observed in DFT calculations (Figure S6).

Thus, the combination of the vertical dipole moment located within the helix and soft vibrational mode provides optimal conditions for the converse piezoelectric response. To explore this aspect of the 7HdiET molecule, we recorded frequency shift maps $\Delta f(z,V_B)$ as a function of the tip−sample distance z and applied sample bias V_B (see Figure 4). Using the contacting distance z_c (a distance at which the $\Delta f(z,V_B)$ minima occur) as a reference, we can track the mechanical deformation of the molecule induced by an applied external electric field with high precision. Figure 4 reveals that z_c varies linearly with the applied bias voltage. At positive sample bias (i.e., tip has a negative effective charge) the tip has to approach closer to the molecule in order to contact it (the molecule is compressed), while at negative sample bias z_c is increased (the molecule is stretched). We found a very similar linear variation of z_c with the applied bias independently of the conformers (see Supplemental Table S1). This suggests that the deformation of the molecule in the electric field is intrinsic to the helicene scaffold rather than to the movement of the acetylsulfanyl group. Also, the orientation of the molecule dipole discussed explains well the experimentally observed molecular deformation induced by the electric field, when the molecule contracts at the positive sample bias (i.e., negatively charged tip apex) and vice versa.

Our $\Delta f(z,V_B)$ spectra reveal a parabolic dependence of the frequency shift (i.e., force) on applied bias, see Figure S7, which cannot explain the linear deformation. Thus, we attribute it to a vertical linear relaxation of the helical scaffold (altering the helix pitch) under the applied bias. Indeed, this is supported by the DFT calculations with applied external electric field (see Figure S14) showing a dominant vertical relaxation in the helix. We should note that calculated molecular deformations are 1 order

DOI: 10.1021/jacs.7b08729
J. Am. Chem. Soc. 2018, 140, 940−946

of magnitude lower than those observed experimentally. We attribute this discrepancy to inherent problems to describe properly charge transfer at organometallic interfaces and their polarization. Second, in the experiment the electric field can be enhanced locally by presence of metallic tip (as in, e.g., tip-enhanced Raman spectroscopy). Therefore, we cannot expect the perfect agreement between the magnitude of deformation obtained from DFT calculations and the experiment.

It is also worth noting that we detected a very similar slope $z_c(V_B)$ for the bright and dark conformers, while the tunneling current was very different (see Figure 3b). This supports the conclusion that the PE observed is not affected by any cross-talk between the frequency shift and tunneling current channels.[36]

The piezoelectric constant d_{33} of the molecule 7HdiET can be estimated from the linear slope $z_c(V_B)$ as follows:

$$d_{33} = \frac{\Delta z(E)}{z_o} \times \frac{1}{E}$$

where Δz is a change in the molecular length for a given applied electric field E and z_o represents the molecular length at the zero-electric field. In fact, the electric field E is a priori unknown in the experiment. Nevertheless, in a limiting case, assuming a perfect screening of the applied bias in metals and its linear decay in the molecular junction, we can estimate the electric field in the junction as $E = V_B/z_{ts}$, where z_{ts} is the distance between the metallic surface and tip apex obtained from the DFT calculations[37−39] (see Figure S1) and V_B is the applied sample bias. Adopting this approximation, we estimate the average piezoelectric constants d_{33} for the bright and dark conformers as 54 and 53 pm/V, respectively. We obtained very similar results for different molecules during different sessions (see Figure S15). Lacking experimental values for single molecules, we compare these values to polymers (e.g., PVDF: 33 pm/V), inorganic materials such as ZnO (e.g., 4−12 pm/V) or biological materials such as thin films of bacteriophage (e.g., 8 pm/V). However, we should note that in the present experiments single molecules are exposed to much larger electric field than those typically applied in in traditional mesoscopic PE materials.

We also measured the electromechanical response of the molecule 7HdiT that shares the heptahelicene scaffold with the molecule 7HdiET, but is functionalized with the native sulfanyl groups instead of acetylsulfanyl (see Supplementary Discussion and Figure S16). Similarly to 7HdiET, it is possible to contact the molecule 7HdiT and measure the corresponding $\Delta f(z,V_B)$ maps. Even though the molecule 7HdiT interacts differently with the scanning probe tip than 7HdiET, it is still possible to reproducibly contact the molecule 7HdiT within the range of ±0.8 V of the sample bias voltage. The acquired $\Delta f(z,V_B)$ spectra on the molecules 7HdiT reveal a significant converse piezoelectric effect as well, having a slightly larger value of 80 pm/V of the d_{33} coefficient than found at the bright and dark conformers of 7HdiET ∼ 50 pm/V.

Let us summarize a possible origin of the strong converse piezoelectric response of the racemic heptahelicene derivatives. The molecule 7HdiET in gas phase does not possess any significant vertical dipole moment aligned with the helix axis because of its C_2 symmetry. Thus, at first glance it seems to be disqualified as a candidate for single-molecule PE. However, once deposited on a metallic surface, its C_2 symmetry is broken to form a C_1 symmetric adsorbate lacking the inversion symmetry. On top of this, the charge transfer from the molecule to surface creates the vertical dipole within the molecule helix, which coupled to the helix soft vibrational mode provides strong PE. This scenario holds for both enantiomeric *M* and *P* forms of helicenes. Therefore, the PE effect is independent of molecular chirality. We should note that changes in the molecular tilt angle induced by the applied electric field would result in a similar electromechanical deformation as reported here. While we cannot completely rule this scenario out, there are several arguments based on measurements and simulations (detailed in Supporting Information) disfavoring this interpretation.

In addition, we performed a control measurement on isolated thiol-functionalized *o*-carborane CBdiT molecules. They consist of a compact core of covalently linked boron and carbon atoms (Figure S17). Therefore, the electromechanical deformation may only take place in thiol bonds on the interface between the molecule and surface. The compact character of the molecular core and presence of two thiol bonds also minimize the possibility of any molecular tilt or rotation. The acquired $\Delta f(z)$ curves show different character than those acquired on helicene molecules. Namely, we do not observe the characteristic jump to the contact observed in helicenes, but a gradual decrease of the frequency shift upon tip approach. This behavior is very similar to that observed in single atomic metallic contacts (see, e.g., ref 46). This striking difference in the $\Delta f(z)$ spectra indicates a distinct mechanical response of *o*-carborane and helicene molecules. The rigid internal structure of the *o*-carborane does not allow any sudden jump to the contact, while for helicenes the presence of the soft helix mode does.

The measured electromechanical linear response of CBdiT was ∼10 pm/V. Though not negligible, this value is at least three times lower than for helicenes ($\gtrsim$ 30 pm/V). These results reveal, on one hand, that thiolate bonds may experience some electromechanical deformation too but, on the other hand, that the helical scaffold plays an important role in enhancing the molecular piezoelectric response. This helical structure brings soft vibrational modes where the molecule is deformed along the axis of the helix.

Importantly, there is significant room for the further enhancement of the single-molecule (converse) PE either by increasing the piezoelectric coefficient of the molecule (cf. ref 29) or by varying the surface workfunction to increase the charge transfer between the molecule and metal (i.e., the vertical dipole). The existence of the single-molecule converse PE indicates that the single-molecule direct PE effect could also be realized as these effects are complementary and reversible. The first experimental observation of the converse single-molecule PE introduces a new concept into the bottom-up design of new molecular nanoelectromechanical devices such as actuators, sensors or electricity generators. Not only polarized molecules on the metallic surface reported here but also isolated dipolar molecules,[29] as analyzed by Hutchison,[32] may constitute diverse PE materials at nano-, micro- or macroscale. In particular, the so far neglected PE molecule-elastomer hybrid materials are envisaged to find meaningful applications in downsized soft robotics[42,43] complementing, for instance, dielectric electroactive elastomers[44] but enabling much lower driving voltages.[45]

3. CONCLUSIONS

In this work, we investigate the piezoelectric effect in single helicene molecules on Ag(111) surface, using simultaneous

DOI: 10.1021/jacs.7b08729
J. Am. Chem. Soc. 2018, 140, 940−946

noncontact AFM and STM measurements. The helicene on the substrate forms circular and linear islands, which can be effectively disassembled to individual molecules by the AFM tip, to exclude collective influence on the piezoelectric measurements. We performed the bias-dependent $\Delta f(z,V_B)$ spectroscopy, which reveals the strong linear shift of the contact distances with applied bias. We attributed the linear bias-induced deformations of the helicene to the piezoelectric response of the molecule. In addition, we found that the piezoelectric response is independent of the acetylsulfanyl group conformation and that it is free from cross-talk artifacts. We corroborated the experimental evidence by the total energy DFT simulations. The calculations reveal strong charge transfer between the helicene molecule and the metallic substrate, which gives rise to a vertical electric dipole across the molecule. The presence of the electric dipole coupled with a soft vibrational mode inherent to the helical structure of the molecule originates the strong piezoelectric effect. The role played by the helical structure in amplifying the electromechanical response was evidenced from control experiments on rigid thiol-functionalized *o*-carborane molecules. The presence of a smaller but still non-negligible electromechanical response in the CBdiT molecules points to the importance of the electromechanical phenomenon in molecular junctions. We believe that the presented data can stimulate further investigation of the electromechanical response in molecular junction and the exploitation of this effect for the design of new molecular machines.

4. METHODS

Heptahelicene derivatives (*S*,*S*′-heptahelicene-2,17-diyl diethanethioate, 7HdiET and heptahelicene-2,17-dithiol, 7HdiT) were synthesized using the procedure described in Supporting Information. The molecules were evaporated under ultrahigh vacuum (UHV, 3×10^{-10} mbar) from a tantalum crucible at ∼350 K (heptahelicene derivatives) or ∼400 K (*o*-carboranes) onto the atomically clean Ag(111) single-crystal surface at ∼350 K. The imaging and spectroscopies of the individual molecules were performed by high-resolution noncontact atomic force microscopy (nc-AFM) and scanning tunneling microscopy (STM) under UHV at low temperature (5 K) using a commercial microscope (SPECS Surface Nano Analysis GmbH) with simultaneous force/current detection capabilities. Prior to the experiments, the probe tip was repeatedly poked into the Ag(111) surface (usually at least 10 nm away from any closest molecular islands) applying 0−3 V bias pulses until a good tip termination capable of molecule contacting was obtained. The optimized structures of molecules on Ag(111), and their interaction with metallic probe were calculated by the FHI-AIMS program packages[37] based on ab initio density functional theory (DFT).[38,39] Electron transport calculations were carried out using the TransSiesta code[34,35] (for details, see Supplementary Methods).

■ ASSOCIATED CONTENT

Supporting Information

The Supporting Information is available free of charge on the ACS Publications website at DOI: 10.1021/jacs.7b08729.

Crystal data (CIF)

Figures S1−S18 with additional discussion, Table S1, and synthesis of molecules 7HdiET and 7HdiT (PDF)

■ AUTHOR INFORMATION

Corresponding Authors

*stary@uochb.cas.cz

*pavel.jelinek@fzu.cz

ORCID

Pavel Jelínek: 0000-0002-5645-8542

Notes

The authors declare no competing financial interest.

■ ACKNOWLEDGMENTS

We thank T. Baše for providing with us the *o*-carborane CBdiT molecules. This work was financially supported by a Czech Science Foundation grants (17-24210Y, 16-08327S, 15-19672S and 14-374527G) and by the Institute of Organic Chemistry and Biochemistry, Czech Academy of Sciences (RVO: 61388963). H.V. gratefully acknowledges financial support from the Purkyně Fellowship program of the Czech Academy of Sciences. We thank the National Grid Infrastructure MetaCentrum and the "Projects of Large Research, Development, and Innovations Infrastructures" CESNET LM2015042 and LM2015087. P.J. acknowledges support of the Czech Academy of Sciences through Praemium Academiae award.

■ REFERENCES

(1) *Advanced Piezoelectric Materials, Science and Technology*; Uchino, K., Ed.; Woodhead Publishing: Cambridge, 2017.

(2) Zhu, H.; Wang, Y.; Xiao, J.; Liu, M.; Xiong, S.; Wong, Z. J.; Ye, Z.; Ye, Y.; Yin, X.; Zhang, X. *Nat. Nanotechnol.* **2015**, *10*, 151−155.

(3) Wu, W.; Wang, L.; Li, Y.; Zhang, F.; Lin, L.; Niu, S.; Chenet, D.; Zhang, X.; Hao, Y.; Heinz, T. F.; Hone, J.; Wang, Z. L. *Nature* **2014**, *514*, 470−474.

(4) Nguyen, T. D.; Nguyen, T. D.; Deshmukh, N.; Nagarah, J. M.; Kramer, T.; Purohit, P. K.; Berry, M. J.; McAlpine, M. C. *Nat. Nanotechnol.* **2012**, *7*, 587−593.

(5) Minary-Jolandan, M.; Bernal, R. A.; Kuljanishvili, I.; Parpoil, V.; Espinosa, H. D. *Nano Lett.* **2012**, *12*, 970−976.

(6) Wang, Z. L.; Song, J. *Science* **2006**, *312*, 242−246.

(7) Fukada, E. Q. *Q. Rev. Biophys.* **1983**, *16*, 59−87.

(8) Farrar, D.; Farrar, D.; Ren, K.; Cheng, D.; Kim, S.; Moon, W.; Wilson, W. L.; West, J. E.; Yu, S. M. *Adv. Mater.* **2011**, *23*, 3954−3958.

(9) Lee, B. Y.; Zhang, J.; Zueger, C.; Chung, W. J.; Yoo, S. Y.; Wang, E.; Meyer, J.; Ramesh, R.; Lee, S. W. *Nat. Nanotechnol.* **2012**, *7*, 351−356.

(10) Masmanidis, S. C.; Masmanidis, S. C.; Karabalin, R. B.; De Vlaminck, I.; Borghs, G.; Freeman, M. R.; Roukes, M. L. *Science* **2007**, *317*, 780−783.

(11) Craighead, H. G. *Science* **2000**, *290*, 1532−1535.

(12) Elbing, M.; Ochs, R.; Koentopp, M.; Fischer, M.; von Hänisch, C.; Weigend, F.; Evers, F.; Weber, H. B.; Mayor, M. *Proc. Natl. Acad. Sci. U. S. A.* **2005**, *102*, 8815−882.

(13) Park, H.; Park, J.; Lim, A. K.; Anderson, E. H.; Alivisatos, A. P.; McEuen, P. L. *Nature* **2000**, *407*, 57−60.

(14) Perrin, M. L.; Frisenda, R.; Koole, M.; Seldenthuis, J. S.; Celis Gil, J. A.; Valkenier, H.; Hummelen, J. C.; Renaud, N.; Grozema, F. C.; Thijssen, J. M.; Dulić, D.; van der Zant, H. S. J. *Nat. Nanotechnol.* **2014**, *9*, 830−834.

(15) Reddy, P.; Jang, S. Y.; Segalman, R. A.; Majumdar, A. *Science* **2007**, *315*, 1568−1571.

(16) Zheng, X.; Mulcahy, M. E.; Horinek, D.; Galeotti, F.; Magnera, T. F.; Michl, J. *J. Am. Chem. Soc.* **2004**, *126*, 4540−4542.

(17) Tierney, H. L.; Murphy, C. J.; Jewell, A. D.; Baber, A. E.; Iski, E. V.; Khodaverdian, H. Y.; McGuire, A. F.; Klebanov, N.; Sykes, E. C. H. *Nat. Nanotechnol.* **2011**, *6*, 625−629.

(18) Leigh, D. A.; Wong, J. K.; Dehez, F.; Zerbetto, F. *Nature* **2003**, *424*, 174−179.

(19) Kelly, T. R.; Silva, R. A.; Silva, H. D.; Jasmin, S.; Zhao, Y. A. *J. Am. Chem. Soc.* **2000**, *122*, 6935−6949.

(20) Koumura, N.; Zijlstra, R. W.; van Delden, R. A.; Harada, N.; Feringa, B. L. *Nature* **1999**, *401*, 152−155.

(21) Erbas-Cakmak, S.; Leigh, D. A.; McTernan, C. T.; Nussbaumer, A. L. *Chem. Rev.* **2015**, *115*, 10081−10206.

(22) Bruns, C. J.; Stoddart, J. F. *Acc. Chem. Res.* **2014**, *47*, 2186−2199.
(23) Kudernac, T.; Ruangsupapichat, N.; Parschau, M.; Maciá, B.; Katsonis, N.; Harutyunyan, S. R.; Ernst, K. H.; Feringa, B. L. *Nature* **2011**, *479*, 208−211.
(24) Shirai, Y.; Osgood, A. J.; Zhao, Y.; Kelly, K. F.; Tour, J. M. *Nano Lett.* **2005**, *5*, 2330−2334.
(25) Chen, C. F.; Shen, Y. *Helicene Chemistry: From Synthesis to Applications*; Springer-Verlag: Berlin, 2017.
(26) Šesták, P.; Wu, J.; He, J.; Pokluda, J.; Zhang, Z. *Phys. Chem. Chem. Phys.* **2015**, *17*, 18684−18690.
(27) Guo, Y. D.; Yan, X. H.; Xiao, Y.; Liu, C. S. *Sci. Rep.* **2015**, *5*, 16731.
(28) Vacek, J.; Chocholoušová, J. V.; Stará, I. G.; Starý, I.; Dubi, Y. *Nanoscale* **2015**, *7*, 8793−8802.
(29) Rulíšek, L.; Exner, O.; Cwiklik, L.; Jungwirth, P.; Starý, I.; Pospíšil, L.; Havlas, Z. *J. Phys. Chem. C* **2007**, *111*, 14948−14955.
(30) Rempala, P.; King, B. T. J. *J. Chem. Theory Comput.* **2006**, *2*, 1112−1118.
(31) Jalaie, M.; Weatherhead, S.; Lipkowitz, K. B.; Robertson, D. *Electron. J. Theor. Chem.* **1997**, *2*, 268−272.
(32) Quan, X.; Marvin, C. W.; Seebald, L.; Hutchison, G. R. *J. Phys. Chem. C* **2013**, *117*, 16783−16790.
(33) Kitagawa, K.; Morita, T.; Kimura, S. A. *Angew. Chem., Int. Ed.* **2005**, *44*, 6330−6333.
(34) Soler, J. M.; Artacho, E.; Gale, J. D.; García, A.; Junquera, J.; Ordejón, P.; Sánchez-Portal, D. *J. Phys.: Condens. Matter* **2002**, *14*, 2745.
(35) Brandbyge, M.; Mozos, J. L.; Ordejón, P.; Taylor, J.; Stokbro, K. *Phys. Rev. B: Condens. Matter Mater. Phys.* **2002**, *65*, 165401.
(36) Majzik, Z.; Setvín, M.; Bettac, A.; Feltz, A.; Cháb, V.; Jelínek, P. *Beilstein J. Nanotechnol.* **2012**, *3*, 249.
(37) Blum, V.; Gehrke, R.; Hanke, F.; Havu, P.; Havu, V.; Ren, X.; Reuter, K.; Scheffler, M. *Comput. Phys. Commun.* **2009**, *180*, 2175−2196.
(38) Perdew, J. P.; Burke, K.; Ernzerhof, M. *Phys. Rev. Lett.* **1996**, *77*, 3865.
(39) Tkatchenko, A.; Scheffler, M. *Phys. Rev. Lett.* **2009**, *102*, 073005.
(40) Koch, N. *ChemPhysChem* **2007**, *8*, 1438−1455.
(41) Ishii, H.; Sugiyama, K.; Ito, E.; Seki, K. *Adv. Mater.* **1999**, *11*, 605−625.
(42) Rus, D.; Tolley, M. T. *Nature* **2015**, *521*, 467−475.
(43) Ilievski, F.; Mazzeo, A. D.; Shepherd, R. F.; Che, X.; Whitesides, G. M. *Angew. Chem., Int. Ed.* **2011**, *50*, 1890−1895.
(44) Keplinger, C.; Sun, J. Y.; Foo, C. C.; Rothemund, P.; Whitesides, G. M.; Suo, Z. *Science* **2013**, *341*, 984−987.
(45) Carpi, F.; Bauer, S.; De Rossi, D. *Science* **2010**, *330*, 1759−1761.
(46) Ternes, M.; Gonzalez, C.; Lutz, C. P.; Hapala, P.; Giessibl, F. J.; Jelinek, P.; Heinrich, A. J. *Phys. Rev. Lett.* **2011**, *106*, 016802.

DOI: 10.1021/jacs.7b08729
J. Am. Chem. Soc. 2018, 140, 940−946